Macroscopic Mixing in Fluidization

E. J. CAIRNS and J. M. PRAUSNITZ

University of California, Berkeley, California

Mixing studies were performed in beds of lead and glass particles fluidized with water. A salt solution was injected from a point source, and electrical conductivity cells were used to determine time average and fluctuating salt concentrations at various points downstream from the point of injection. The frequency distribution of the fluctuations was determined, and correlation coefficients were measured for the fluctuations at two points separated by a known distance.

The mixing data for the central portion of the bed yield radial eddy diffusivities and scales and intensities of turbulence. At the same fraction void the eddy diffusivity and scale of turbulence are larger for lead than for glass particles, but the velocity fluctuations appear to be independent of the density of the particles. Minimum Peclet numbers are observed at a fraction void of about 0.7. Scales based on correlation coefficients exceed those calculated from Peclet numbers, indicating that in a fluidized bed there are large-scale eddies whose size is much larger than a particle diameter. The interpretation of the mixing data is coupled with visual observations of fluidized bed flow patterns.

During the past few years there has been increased activity in research leading to a more basic understanding of mixing processes in moving fluids. Mixing in gas-fluidized beds was investigated by Gilliland and Mason (*8, 9*) who observed very low Peclet numbers indicating very rapid mixing in the fluid phase. Bernard and Wilhelm (*2*) investigated radial mixing in packed beds for both gaseous and liquid systems; these studies were extended to liquid-fluidized beds by Hanratty, Latinen, and Wilhelm (*10*) who presented results of several sets of experiments using spheres of silica and glass fluidized by water. On the basis of the turbulent-diffusion approach suggested by Taylor (*18, 19, 20*) Hanratty, Latinen, and Wilhelm showed that the concept of a constant eddy-diffusion coefficient only applies after a suitable period of time, or after a suitable distance away from the origin has been attained.

Wilde (*21*) studied the motion of individual glass spheres in a fluidized bed by use of a fluid having the same refractive index as that of the glass beads. The motion of colored tracer beads was then observed. Wilde concluded that the bead motion was not truly random; wavelike motions of bead groups as well as other well-defined circulation patterns were noted.

Recently experimental results on velocity profiles (*4*) and longitudinal eddy diffusivities (*5*) have been reported for liquid-fluidized beds. These studies clearly show that in water-fluidized systems there exist velocity nonuniformities which vary statistically with time, giving rise to axial as well as radial eddy transport within the system. Ordinarily it is convenient to think in terms of a single eddy size as being characteristic of a system of interest. However in a fluidized system a more complete description is given by employing additional characterizing parameters.

It is the aim of this work to contribute to a more complete understanding of the mixing behavior in the liquid phase of liquid-solid fluidized systems. To this end the average or over-all apparent mixing properties in the radial direction, as well as the local fluctuating behavior of the system, have been investigated. Frequency distribution and correlation coefficients of concentration fluctuations have been determined.

THEORY

Mixing-length theory suggests that it is useful to look upon the mixing process in a fluidized bed as analogous to that of molecular diffusion and to write corresponding mass transfer equations which, in steady state experiments, apply well after a sufficient distance from the origin of the system has been reached. When applied to a steady state flow system in a tube, as was used in this work, the mass transfer equation describes the time-average behavior of the system. The differential equation in cylindrical coordinates is

$$E_r\left[\frac{\partial^2\overline{C}}{\partial r^2}+\frac{1}{r}\frac{\partial\overline{C}}{\partial r}\right]+E_z\frac{\partial^2\overline{C}}{\partial Z^2}-U\frac{\partial\overline{C}}{\partial Z}=0 \qquad (1)$$

Equation (1) assumes symmetry about the axis. The solution to this differential equation has been given considerable attention (*2, 10, 11, 13, 14, 17, 20*). If one makes the very good assumption (*14*) that the longitudinal diffusion contribution to mass transfer is small compared with the convective flow term, then the concentration profile for the spreading of mass from a point source (located at $r = z = 0$) is

$$\frac{\overline{C}}{C_\infty}=\frac{N_{Pe,r}\left(\frac{r_o}{d_p}\right)^2}{4\left(\frac{Z}{d_p}\right)}\cdot$$

$$\exp\left[\frac{N_{Pe,r}\left(\frac{r}{d_p}\right)^2}{4\left(\frac{Z}{d_p}\right)}\right] \qquad (2)$$

Equation (2) is limited to the central section of the tube where U is constant and for mathematical reasons to the region $Z/r > 5$.

Visual observations on liquid-solid fluidized beds made in this work and by previous investigators (*21*) indicate the presence of over-all circulation patterns which are due to changes in fluid velocity as the wall is approached. This observation is confirmed by velocity-profile data (*3, 4*) which show that the velocity is very nearly constant for the region $r = 0$ to $r = 0.25\,r_o$ and then falls at points farther removed from the center. Although data at larger radial distances were taken in this work, only those data restricted to the region $0 \leq r/r_o \leq 0.25$ were reduced by Equation (2).

Equation (2) expresses the time-average behavior of the system in terms of time-average concentrations as a function of position in the bed. To obtain a more extensive picture of the mixing behavior and to characterize it in a more detailed and accurate manner interest is directed to the fluctuating concentration behavior in the bed, in addition to the time-average values. A relationship between the concentration fluctuations and the flow parameters characterizing turbulence is needed to give consistency to the connection between ideas relating to turbulence on one hand and turbulent mixing and mass transfer phenomena on the other. Knowledge concerning such a relationship is still far from complete (*12*). However Prausnitz and Wilhelm (*17*) considered this problem in connection with packed-bed studies and proposed a fluid-displacement model wherein the instantaneous concentration at any point in the system is equal to the time-average concentration at some other point. For the root-mean-square fluctuating concentration they obtained

$$\frac{\sqrt{\overline{c'^2}}}{\overline{C}}=\frac{\sqrt{2}\frac{\sigma_r r}{d_p^2}}{m^2}=\frac{\sigma_r}{\sqrt{2}\,d_p}\frac{\partial\ln\left(\frac{\overline{C}}{C_\infty}\right)}{\partial\left(\frac{r}{d_p}\right)} \qquad (3)$$

E. J. Cairns is now at the General Electric Research Laboratories, Schenectady, New York.

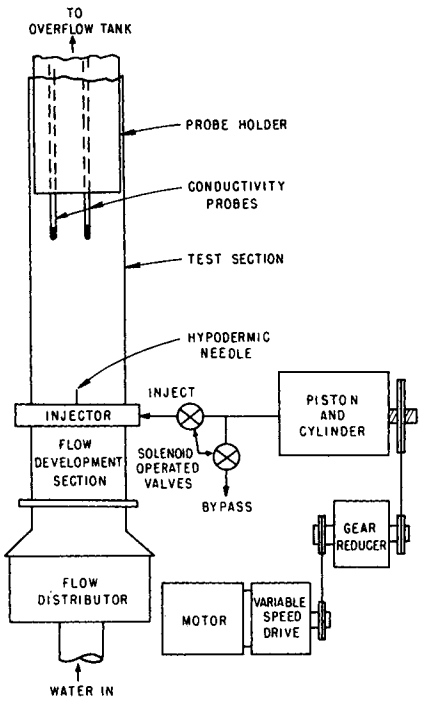

Fig. 1 Schematic flow diagram.

Equation (3) holds for radial locations not too near the center, nor too near the wall, and at longitudinal locations well removed from the point source. It shows the interesting result that the magnitude of the concentration fluctuation depends primarily on the scale of turbulence and not upon the intensity, under the limitations given above.

In accordance with the mixing-length theory the eddy diffusivity is equal to the product of the scale of turbulence, which is assumed to be σ_r, and the root-mean-square value of the velocity fluctuation. Thus

$$E_r = \sigma_r \sqrt{\overline{v'^2}} \qquad (4)$$

$$\frac{1}{N_{Pe,r}} = \frac{\sigma_r}{d_p} \frac{\sqrt{\overline{v'^2}}}{U} \qquad (5)$$

From time-average mixing data and from fluctuation studies independent measurements of E_r and σ_r may be made, allowing the calculation of $\sqrt{\overline{v'^2}}$.

When one now considers the relationship of concentration fluctuations at a point in the system to the concentration fluctuations at another point separated from the first, it is useful to define a concentration fluctuation correlation coefficient, which is somewhat analogous to the correlation coefficient used in connection with Danckwerts' treatment of segregation (6). Such a correlation coefficient is

$$R_c \equiv \frac{\overline{c'_1 c'_2}}{\sqrt{\overline{c'^2_1}}\sqrt{\overline{c'^2_2}}} \qquad (6)$$

By defining the correlation coefficient in this way it is found to have more general applicability than the Danckwerts correlation coefficient associated with segregation, since in the definition used here the system is not required to possess an absence of large-scale segregation. This is true because in Equation (6) the normalization factor $\sqrt{\overline{c'^2_1}}\sqrt{\overline{c'^2_2}}$ is not a constant for the system as a whole but is composed of properties of the points of interest only.

In general R_c has the properties

$$\left(\frac{\partial R_c}{\partial s}\right)_{s=0} = 0$$

$$R_c(0) = 1$$

$$R_c(\infty) = 0$$

If the two points of observation are within a distance less than the size of a packet of fluid which is approximately homogeneous with respect to concentration, then one would reasonably expect to have a positive correlation coefficient. As the distance of separation becomes infinitesimally small, R_c would be expected to approach unity. As the two observation points are separated to the point where they are at a distance greater than the size of the isoconcentration packet, a nonpositive value of R_c would be expected.

As shown by Danckwerts (6) the concentration fluctuation correlation coefficient must have a gradient of zero at $s = 0$ if molecular diffusion is present in the system.

The scale of concentration fluctuation is defined as

$$\lambda = \int_0^\infty |R_c|\, ds \qquad (7)$$

This scale may be thought of as being characteristic of the size of a packet of fluid which is approximately homogeneous with respect to concentration. This is analogous to the conventional scale of turbulence (or scale of velocity fluctuation) in that the conventional scale of turbulence characterizes the size of a packet of fluid, all of which have the same velocity.

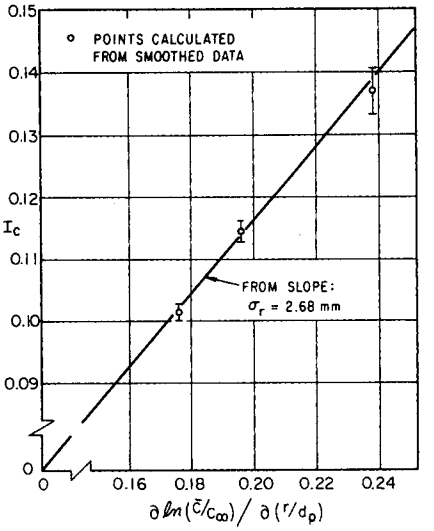

Fig. 3. Determination of scale in a 4-in. tube with 3.196-mm. glass spheres (ϵ = 0.617).

R_c may at some distance α along the s axis pass through zero and take on negative values. At some larger distance β along the s axis R_c must return to zero again. A number of such oscillations may take place, depending on the mixing behavior of the system. Since a portion of the area under the R_c curve may be negative, λ is defined in Equation (7) so that the absolute value of each area is added.

Some rather interesting conclusions may be drawn from a knowledge of the R_c curve and/or the values of λ, as well as the positive and negative contributions to λ. Therefore λ is broken into its components:

$$\lambda = \lambda_0 + \lambda_1 + \ldots \qquad (8)$$

where

$$\lambda_0 \equiv \int_0^\alpha R_c ds \qquad (9)$$

$$\lambda_1 \equiv \int_0^\beta |R_c| ds \quad \text{etc.} \qquad (10)$$

The parameter α is the distance between points in the system where there ceases to be a positive correlation between the concentration fluctuations. At a distance of separation greater than α and less than β there is a negative correlation, which is characteristic of vortex fluid motion.

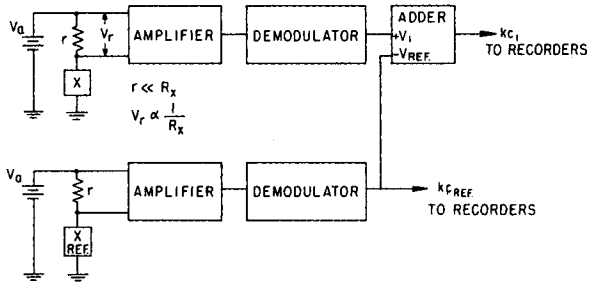

Fig. 2. Block diagram of single channel.

EXPERIMENTAL

Fluctuations in concentration, which may reach a frequency in the range of hundreds of cycles per second, can only be measured by an instrument having a very short time constant. Such an instrument is an elec-

trical conductivity cell coupled with suitable electronic apparatus.

Mixing studies were made by injecting sodium nitrate solution from a point source into a water stream which is used to fluidize the solid particles. A schematic flow diagram is shown in Figure 1.

Electronics

It is possible to obtain a potential which is directly proportional to the electrical conductance of the circuit element in question by use of a simple circuit as shown in Figure 2. By operating in a frequency range of 20 kc. polarization effects are eliminated, and good demodulation up to 400 cycles per second of signal is easily attained (*3*). By proper selection of the size of resistor r in Figure 2 a signal V_r is obtained which approaches direct proportionality to the conductivity L_x. In the concentration range studied in the present experiments the conductance of the sodium nitrate solutions used is directly proportional to the concentration of sodium nitrate. For this work r was selected so that it was only 1% as large as the smallest value of R_x which was encountered.

The voltage V_r was amplified and demodulated, yielding a signal which reflects exactly the conductance behavior of the conductivity cell. Use of an adding circuit allowed the signal of a reference conductivity cell placed in the water stream entering the test section to be subtracted from the signal of the cell measuring the salt solution conductance in the test section (see Figure 2). The amplifier demodulator was constructed so that six conductance signals in parallel could be observed.

Blocking condensers applied to the output signal of the amplifier-demodulator system yield a signal which is proportional to the fluctuating component of the concentration. A simple R-C filter network allows an average value of the signal from the amplifier demodulator to be measured. A true root-mean-square voltmeter was used to determine the root-mean-square value of the fluctuating component of concentration. Continuous multiplication of signals having frequency components up to 470 cycles per second was effected by employing an analogue computer. All amplifiers in the system were linear to within less than 1%. A waveform analyzer was used to obtain the frequency spectrum of the concentration fluctuations. A visicorder gave a continuous record of all instantaneous concentrations.

Conductivity Probes

The conductivity cell proper was made from a slotted 3-mm. diameter rod, having 0.050-in. diameter circular platinum electrodes mounted 1 mm. apart. The slot in the rod is 7 mm. deep, thus allowing the stagnation point of the fluid impinging at the base of the slot to be at such a distance from the electrodes that its influence on the measurements would be negligible.

The probe was constructed by drilling a 0.05-in. hole perpendicular to the axis of the rod, about 2 mm. from one end. A piece of 0.05-in. platinum wire was sealed firmly in the hole, and 32-gauge copper wires were attached to the ends of the platinum wire. The copper wires were sealed into axial depressions along the outside of the rod and were secured by epoxy resin. The rod was then slotted so that the platinum wire was cut perpendicular to its axis, thus exposing two 0.05-in. diameter circular electrodes facing one another and 1 mm. apart. The exposed end of the rod is hemispherical in shape causing the probe tip to appear much like a packing particle. The rod containing the electrodes is about 2 cm. long and is mounted at the end of a ⅛-in. O.D. stainless steel tube so that the copper leads from the electrodes pass through the tube.

The capacitance effects were negligible, and cross talk between probes was always less than 1%. The probe is mounted in a rigid probe holder wherein the radial position of the probe may be selected at intervals of 1/6 of an inch. Angular orientations and axial position may take on any desired values. All observations were made with the probe tip at a distance of about 5-in. from the nearest probe-support member.

The conductivity probes were sufficiently small to enable good observations to be made of fast concentration fluctuations. In most runs the probable upper-frequency limit was around 400 to 500 cycles per second; in no case was it below 250 cycles per second. This lower figure is computed from the characteristic dimension of the cell (1 mm.) and the lowest fluid velocity encountered in this work (250 mm./sec.).

Flow Apparatus

The flow system consisted of a constant head water tank located approximately 35 ft. above the test section, a 5-hp. regenerative turbine pump, a 5-hp. centrifugal pump, a set of five rotameters having a total range of 0.01 to 61 gal./min., a flow distributor, a flow development section, the test section, and an overflow tank connected to a drain.

The entrance to the flow distributor consisted of a capped 2-in. pipe having small lateral holes around the periphery near the cap. The discharge from the peripheral holes entered a conical expansion section covered with a plate having 1/16-in. holes on a triangular arrangement so that the fraction voids was 0.38. The flow then proceeded upward into the flow-development section which consisted of an 8-in.-high section of tube packed with 2-mm. pyrex spheres, covered with a stainless steel screen.

Mounted on top of the flow-development section was the point-source injector, having a screen at about the level of the upper surface of the injector body. The space enclosed by the injector body was also packed with 2-mm. spheres. The point-source injector tube (hypodermic needle in Figure 1) protruded vertically from the uppermost screen a distance of about 5 cm. This distance is sufficiently large to eliminate the effects of the bed entrance (*10*).

The test section consisted of a 3.98-in. I. D. pyrex pipe, 2 ft. high.

Injection System

The 1.0 normal sodium nitrate tracer solution was injected into the test section by means of a piston and cylinder arrangement, the piston being driven by means of a geared-down variable-speed drive unit. The speed of the piston was calibrated accurately against drive settings.

Procedure

The flow rate corresponding to the fraction voids desired was set, and beads were added to or subtracted from the system to give the proper bed height (about 10 in.). The injector-drive setting was adjusted to give a linear speed to the injectant equal to that of the main-stream fluid as calculated from the superficial velocity divided by the fraction voids in the bed. After satisfactory steady state concentration values were reached, the recorders were connected to each of the probes in turn, yielding data on $\overline{C_i}$, $\overline{c'_i{}^2}$ $\overline{c'_i c'_j}$, and $\sqrt{\overline{c'_i{}^2}}/\overline{C_i}$ for each probe.

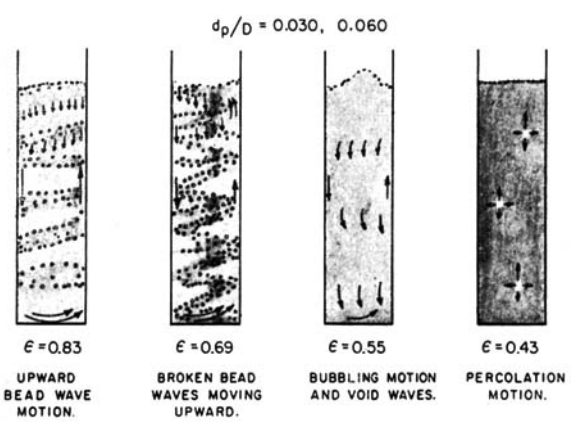

Fig. 4. Fluidization of glass spheres.

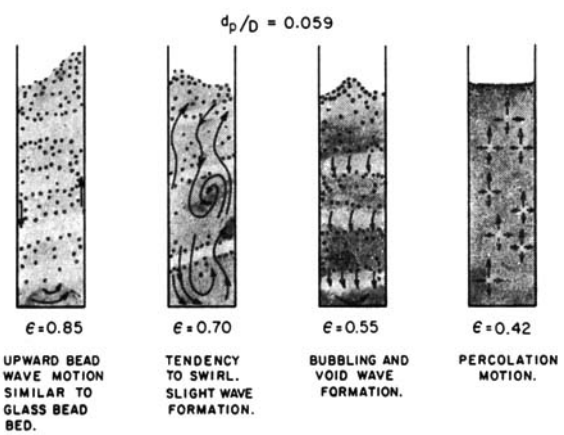

Fig 5. Fluidization of lead spheres.

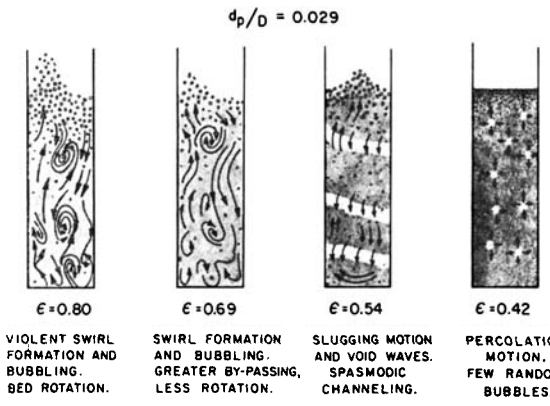

Fig. 6. Fluidization of lead spheres

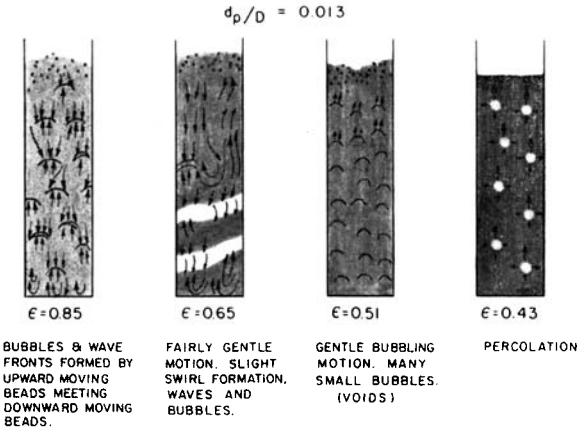

Fig. 7. Fluidization of lead spheres.

A mixed-cup sample of the effluent was taken, and conductivity readings of this sample were taken with each probe.

The flow pattern of the bed was given careful visual observation, and sketches were made of the bed appearance.

REDUCTION OF DATA

Since all of the signals recorded as data are proportional to the conductance of the solution, a conversion from conductance to concentration is necessary. Fortunately in the concentration range used in this work (approximately 10^{-2} normal) the conductance of aqueous sodium nitrate solutions is directly proportional to the concentration. Therefore at any temperature the concentration is given by the equation

$$C = aL \qquad (11)$$

All concentrations and concentration fluctuations are reported in terms of ratios. The ratio of two concentration values is equal to the corresponding ratio of the conductances, and the constant a cancels. Thus the concentration ratios are equal to the voltage ratios measured directly with the apparatus.

Concentration profiles were plotted for the various angular orientations of the probe holder at a given distance from the point source. Because of slight asymmetry the centers of the concentration profiles were determined by the point of highest concentration which is not necessarily the same as the geometric center; details of the asymmetry are given elsewhere (3). All data at a given level were combined on one plot, and reflected points were used to eliminate slight asymmetries. By plotting $\ln(\bar{C}/C_\infty)$ vs. $(r/d_p)^2$ for the central region as determined from the smoothed concentration profiles [see Equation (2)], the Peclet number may be determined from the slope and/or the intercept. Since slight errors in locating the concentration center line can cause relatively large errors in the determination of the Peclet number by the intercept method, only the slope results were used. Peclet groups were computed only from smoothed data for the region $0 \leq r/r_o \leq 0.25$.

The frequency distribution of the fluctuating components of concentration was determined as a function of fraction voids. Since the magnitude of the concentration fluctuation depends on position in the bed [see Equation (3)], it is desirable to plot the data taken at various positions in the bed in such a manner that they may be easily compared. For this reason the data from the wave analyzer were made dimensionless through division by the corresponding true root-mean-square voltmeter readings. If the true root-mean-square meter had exactly the same frequency-response characteristics as the wave analyzer, then the area under each frequency-analysis curve would be unity. The two instruments have different low frequency cut-off response curves, and hence the area is not unity.

Since the concentration-fluctuation magnitude depends on the time average concentration gradient, and since this gradient varies with bed expansion as well as with position in the bed, results from one run to the next are rather difficult to compare if one attempts to consider only the magnitude of the concentration fluctuation, or the value of the ratio of $\sqrt{\overline{c'^2}}(f)$ (determined at frequency f) to $\sqrt{\overline{c'^2}}_{\text{RMS meter}}$ which measures the fluctuations summed over all frequencies. The observed frequency curves appear to consist of two portions, one characteristic of the fluid flow independent of particle motion and the other characteristic of fluid behavior as influenced by the fluidized particles. For this reason it was decided to orient the curves from various states of fluidization in such a manner that the high-frequency ends of the curves would extrapolate to roughly the same fluctuation value. This high-frequency end of the curve is independent of the fluidized particle motion; it is characteristic of the turbulent fluid flow and less likely to undergo appreciable shifts with changing fluid velocity.

The data on $\sqrt{\overline{c'^2}}$ as a function of radial position were plotted in the same manner as that used for the time-average concentrations. When smoothed in this manner these curves are symmetrical about a point near $r = 0$. The curves for average concentration and fluctuating concentration as a function of position yield a new plot as shown in Figure 3. From Equation (3) the slope is $(\sigma_r)/(\sqrt{2}\,d_p)$ for points not near the center or near the wall.

From the Peclet numbers and scales of turbulence the intensities of turbulence are calculated by Equation (5).

DISCUSSION OF RESULTS

Visual observations of the particle flow patterns at various d_p/D ratios for glass and lead beads as a function of fraction voids are shown in Figures 4 through 7. Figure 4 shows the observations for glass beads for two d_p/D ratios, and as closely as one can tell visually the patterns of flow and general characteristics are the same for both ratios. Starting at the right-hand side of the diagram there is a slight percolating motion in the range of 43% voids where small void bubbles move randomly up through the bed. As the fraction voids is increased to 0.55 the bubbling motion becomes more predominant and yields to a void-wave formation which causes a gentle slugging and bubbling motion. The particles drop across the void waves to reform another slug. Little over-all circulation is observed. As the fraction voids is increased to 0.69, the void waves disappear, yielding to broken particle waves. This interchange of phases may be thought of as being analogous to a vaporization process in

which the vapor phase is increasing and finally predominates, leaving the liquid phase in the minority. The dense phase is now the discontinuous phase in a continuous dilute phase. Some slow, over-all circulation patterns are detected, as noted by the arrows next to the tube walls. Finally, at fraction voids of about 0.85, a stronger general circulation or swirling pattern is set up; the particle waves are more well defined and contrast well against the dilute phase. The most active local particle motion occurs in the range of $\epsilon = 0.7$.

Figure 5 shows lead particles at a d_p/D ratio of 0.059. At the start of fluidization (the right-hand drawing) the percolation motion exists as with glass particles. Increasing the fraction voids yields bubbles and void waves, as with glass. At fraction voids of about 0.7 there is a more violent motion than with glass and a definite tendency to form swirls and waves, apparently promoting increased mixing. By the time the bed is expanded to fraction voids of about 0.85 the similarity to the glass behavior is restored. All local particle motions are more violent than with glass, even though most of the general bead behavior is preserved.

Turning to Figure 6 at a lower ratio of d_p/D one might expect that the particles have more freedom to move about, and hence swirl formation and more rapid general circulation are to be expected. This is just what is found, especially at higher fraction voids.

Decreasing the d_p/D ratio to 0.013 as in Figure 7 shows that the particles now show more of a tendency to behave as a liquid phase, individual particles tending to lose identity. Bubbling similar to that of a gas through a liquid is detected. Swirling motion is less and various bubble motions predominate.

The expected conclusion reached from visual studies is that two important variables play a part in bed characteristics, particle-to-tube diameter ratio and the density difference or particle-to-fluid density ratio. Most violent motion occurs at $\epsilon \approx 0.7$, where a phase transition is observed. The qualitative results shown in Figures 4 through 7 illustrate some of the differences and similarities between liquid- and gas-phase fluidized beds (*1, 15, 16*).

An analogy between packed and fluidized beds may be a guide to a first attempt at describing the mixing behavior in liquid solid fluidization systems. Peclet numbers adequately describe the mixing phenomena in packed beds and are reported in this work as a starting point for a more detailed analysis of the turbulent mixing behavior.

Peclet numbers calculated from measured time-average concentration profiles at a d_p/D ratio of 0.03 are reported in Figure 8. From the particle flow patterns discussed above one might have predicted the general characteristics shown, that is better mixing (lower Peclet number) in the region of $\epsilon \approx 0.7$ and better mixing with more dense particles at a given fraction voids. The curves extrapolate to packed- and empty-bed values. The results of this work are compared with those of Hanratty, Latinen, and Wilhelm (*10*) for a d_p/D ratio of 0.06, using glass beads.

The analogy to packed-bed behavior for fluidized beds is quite limited, and one should consider a more detailed description and characterization of the liquid-phase mixing. The study of this process immediately reveals a predominant fluctuating behavior of both velocities and concentrations. A study of the fluctuating concentrations must include the frequency analysis of these fluctuations which are summarized in Figure 9.

The general behavior in a packed bed is a frequency distribution characteristic of the flow through the small irregular channels amongst the particles. This corresponds to the frequency range of about 10 to 200 cycles per second having a maximum in the range of 45 cycles per second. As the bed is fluidized, there is superimposed on the packed-bed spectrum a spectrum much lower in frequency and of increasing magnitude with an increase in the fraction voids. Finally at high fraction voids the fluidization frequency distribution is completely dominated by the characteristics imposed by the particle motion. It is to be expected that the distribution shifts back again to higher frequencies and lower amplitudes as the empty-tube system is approached.

The concentration fluctuations studied and described above allow calculation of turbulence parameters which give a more accurate account of the mixing in fluidization. Equations (4) and (5) show that the eddy diffusivity and Peclet number combine the effects of the scale and intensity of turbulence. The concentration-fluctuation data applied to Equation (3) yield a scale of turbulence independent of the Peclet-group determination. Figure 10 summarizes these results. This set of curves brings out the important point that the main difference between the behavior of lead and glass beds is brought about by the influence of the particle density on the scale of turbulence resulting in a higher eddy diffusivity. The radial Peclet-number curve shows a minimum and the radial scale of turbulence curve a maximum at the fraction voids corresponding to the visually observed phase transition. Similar results were

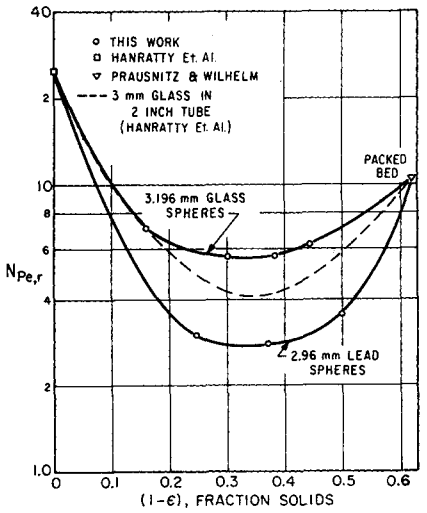

Fig. 8. Radial Peclet groups in fluidization.

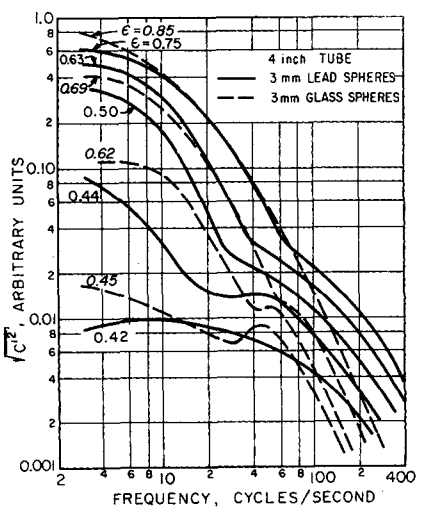

Fig. 9. Concentration fluctuation frequency distribution in fluidization.

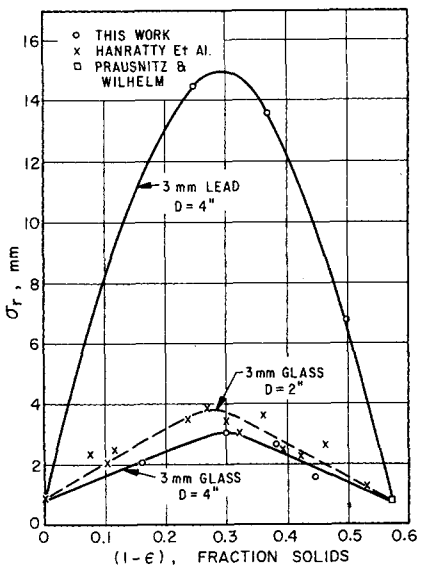

Fig. 10. Scale of turbulence in fluidized beds.

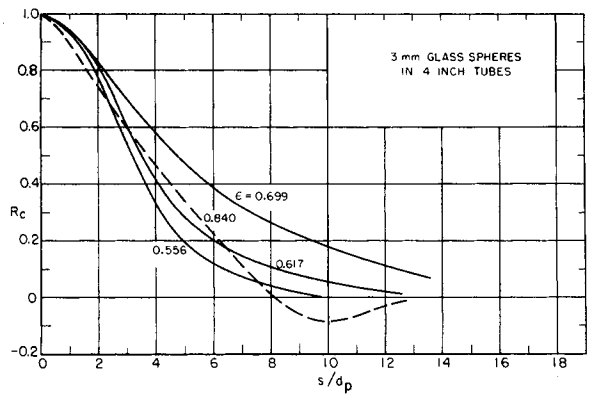

Fig. 11. Concentration fluctuation correlation coefficient vs. distance.

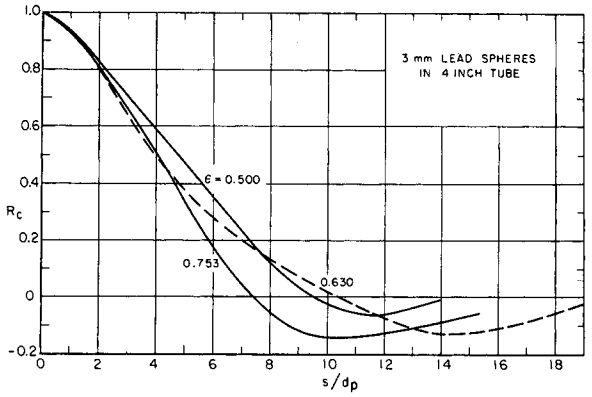

Fig. 12. Concentration fluctuation correlation coefficient vs. distance.

obtained by Lemlich and Caldas (*14a*) who showed that heat transfer to the wall of a fluidized bed reaches a maximum at a fraction void of about 0.7.

An approximate model may be used to explain the particle-density influence on the scale of turbulence. A minimum detectable concentration fluctuation is brought about by the motion of a particle or group of particles having the same minimum momentum M^*. The scale of turbulence is related to and influenced by the mean distance that a particle moves in a given general direction. Any given particle, on the average, loses a certain fraction of its momentum in a single collision. As will be shown later the radial-velocity fluctuations are independent of particle density at given fraction voids. Hence one may reasonably assume that radial velocities of particles are roughly independent of particle density, and the particle momentum is then proportional to the particle density for a given particle size. Plotting the original momentum of a particle, characteristic of the radial-velocity fluctuation in the bed as a starting point, on semilog coordinates vs. the total number of collisions suffered by the particle in question after some reference time, one obtains a straight line, having a slope characteristic of the momentum loss per collision. If the glass and lead beads lose roughly the same fraction of momentum on each collision, then the bead will undergo $[(\rho_{Pb})/(\rho_{glass})]$ times as many collisions as the glass particle before its momentum drops below M^*. This model is tested by comparing the ratios of observed scales of turbulence for 3-mm. lead and glass beads to the density ratio at various fraction voids. The result predicted on the basis of this simple model holds reasonably well; for example at fraction voids of 0.70, $\sigma_{Pb}/\sigma_{glass} = 15/3 = 5.0$ (see Figure 10), while $\rho_{Pb}/\rho_{glass} = 11.3/2.45 = 4.6$.

Using Equation (5) one finds that the intensity of the radial-velocity fluctuations $\sqrt{\overline{v'^2}}/U$ is greater for glass-fluidized beds than for the corresponding lead bed. This result however is somewhat misleading, since the normalizing factor is much greater in the case of lead than in glass. To compare more directly the velocity-fluctuation results Table 1 was prepared, showing the root-mean-square value of the fluctuating component of the velocity as a function of fraction voids for each particle density. This table shows that at the same fraction void the velocity fluctuations are independent of the particle density and that there is a minimum at about $\epsilon = 0.7$. This relatively small trend toward a minimum value is over-shadowed by the much greater effect in the opposite direction shown in the behavior of the scales.

CONCENTRATION FLUCTUATION CORRELATION COEFFICIENTS

Concentration fluctuation correlation coefficients were measured in the central part of the bed by electronic multiplication and the averaging of the AC part of the demodulated signal coming from two electrical conductivity probes placed a known distance apart. In these measurements the two probes were always at the same height above the point-source injector. Since each correlation coefficient is based on measurements made over a large period of time, it was found that the correlation coefficient was independent of the radial positions of the probes but depended only on the distance between probes. Correlation coefficients for glass and lead beads are shown in Figures 11 and 12. In many cases each value which contributed to a curve was the average of several separate determinations. The results shown in the figures were obtained in the central region, that is in the region approximately bounded by $r = 0.5\ r_o$. All measurements were made at a height of 6.025 in. above the point source. The total bed height varied somewhat with fraction void but was always in the range 9.4 to 11 in. Table 2 shows scales calculated from these data with Equations (7), (9), and (10). Figure 11 shows correlation coefficients for glass beads. The maximum distance from the origin experienced by the intercept of one of these R_c curves lies in the range of $\epsilon \approx 0.7$; this is in good agreement with the results for σ_r shown in Figure 10. However the scale of concentration fluctuation defined in Equation (9) and recorded in Table 2 is considerably larger than the scale of turbulence plotted in Figure 10, showing that there is not necessarily any relationship between the conventional Lagrangian scale of turbulence and the scale of concentration fluctuation. One might conceive of a packet of fluid characterized by the scale λ_o having homogeneity with respect to concentration, however containing many isovelocity packets characterized by the scale σ_r. For glass beads the sizes of the two different packets are definitely not the same. For lead, however (see Figure 12) the size of the concentration packet is comparable with that of the velocity packet over portions of the fraction-void range studied.

The values in Table 2 show that the scales based on concentration-fluctuation data are approximately the same for glass- and lead-fluidized beds. This result is in striking contrast with that illustrated by Figure 10 which shows that the scale σ_r for lead is much larger than that for glass. The difference in σ_r is probably related to the fact that

Table 1. Velocity Fluctuations in Fluidization

4-in. tube, 3-mm. spheres

Fluid flow rate, (gal./min.) Glass	Lead	Fraction voids	$\sqrt{\overline{v'^2}}$, (in./sec.) Glass	Lead
—	18.55	0.500	—	1.39
7.43	—	0.557	1.33	—
9.53	—	0.617	0.99	—
—	32.4	0.630	—	1.21
13.05	—	0.699	1.05	—
—	50.0	0.753	—	1.41
21.35	—	0.840	1.70	

to achieve the same fraction voids much more energy must be supplied to a lead-fluidized bed than to a glass-fluidized bed. Scales based on concentration fluctuation correlation coefficients however are probably not very sensitive to the flow velocity but instead depend strongly on the molecular diffusivity of the tracer material in the fluid. It is probable then that these particular results reported here for a liquid-phase bed are quite different from those to be expected for a gas-phase bed.

The positive portion of the R_c curve indicates that at the distance of separation in this region the concentration fluctuations in general behave similarly at the two points of interest, the stronger degree of correlation being reflected in higher values of R_c. It appears reasonable that for the region $R_c > 0$ any two points on the abscissa are in the same concentration packet at the same time. The λ_o values in Table 2 indicate that for the glass system positive contributions to λ are much more sensitive to the fraction voids than are the corresponding contributions in the lead system, but they are roughly the same size for both systems.

The negative correlation coefficient is most likely related to the swirling motion which was observed in the lead-fluidized bed. A possible mechanism leading to a negative R_c may be the following. Consider probes 1 and 2, a distance s apart, where s is larger than the size of an isoconcentration packet. Suppose there are two such packets side by side, one having a concentration higher than the average corresponding to its radial position and the other one lower. One of these packets is in contact with probe 1 and the other with probe 2. There is of course a finite contact time during which each packet is observed by the probes; if, during this contact time, the two packets rotate about their point of contact and change places as a result of swirling, probe 1 will experience negative fluctuation and probe 2 a positive fluctuation, thereby producing a negative correlation coefficient. This mechanism suggests that λ_o is a physically more significant scale than λ.

CONCLUSIONS

1. The mixing properties in a fluidized bed are a strong function of the fraction voids. Minimum values of radial Peclet numbers are observed at $\epsilon = 0.7$, corresponding to a transition in the type of particle circulation in the bed.

2. The packing particle density and fraction voids strongly affect the radial scale of turbulence; larger scales are found for beds containing denser particles at a given fraction voids. The scale of turbulence has a maximum value at $\epsilon = 0.7$.

3. The root-mean-square value of the radial velocity fluctuation varies only slightly with fraction voids and appears to be independent of particle density.

4. The scale of concentration fluctuation is affected by the fraction voids in the same manner as the scale of turbulence, but it is not greatly influenced by the particle density. The scales of concentration fluctuation show that there are isoconcentration eddies several times the size of a packing particle.

5. Studies of concentration fluctuations and their correlation coefficients, coupled with visual observations and time average studies, provide a useful framework for better understanding of macroscopic mixing in fluidized beds.

Table 2. Scale of Concentration Fluctuation

4-in. tube, 3-mm. spheres

Material	Fraction voids	Positive contribution, (mm.)	Negative contribution, (mm.)	Total area, (mm.)
glass	0.556	11.2	0	11.2
glass	0.617	13.5	0	13.5
glass	0.699	18.6	0	18.6
glass	0.840	12.3	0.873	13.2
lead	0.500	13.9	0.974	14.9
lead	0.630	13.9	1.52	15.4
lead	0.753	11.8	2.61	14.4

ACKNOWLEDGMENT

The authors are grateful to Robert L. Sani and William J. Lawrence for assistance in performing the experiments, to F. E. Vogelsberg and to the Lawrence Radiation Laboratory for aid in constructing the electronic apparatus, and to the Standard Oil Company of California for a financial grant.

NOTATION

a = constant in Equation (11), function of temperature
C = concentration of tracer material
C_∞ = mixed cup average concentration of the effluent stream
c' = fluctuating component of concentration as expressed by $C = \overline{C} + c'$
D = test-section diameter
d_p = packing particle diameter
E_r = radial eddy diffusivity
E_z = longitudinal eddy diffusivity
f = frequency, cycles per second
L = conductance
m = $(4Z/d_p)/(N_{Pe,r})^{1/2}$
$N_{Pe,r}$ = radial Peclet group $= (U_o d_p)/(\epsilon E_r)$
r = radial position
r_o = test-section radius
R_C = concentration fluctuation correlation coefficient, defined by Equation (6)
s = distance of separation between probes for determination of R_C
U = fluid velocity, normalizing factor
U_o = superficial fluid velocity
v' = radial component of the fluid-velocity fluctuation
V_a = constant-voltage sine-wave source
X = electrical conductivity cell
Z = longitudinal position

Greek Letters

α = minimum distance between observation points for which R_C is zero
β = minimum distance greater than α between observation points for which R_C is zero
ϵ = fraction voids
λ = scale of concentration fluctuation, defined in Equation (7)
σ_r = radial scale of turbulence as defined in Equation (3)
ρ = density, g/cc.

Subscripts

i, j = probe-position numbers

LITERATURE CITED

1. Bakker, P. J., and P. M. Heertjes, *Brit. Chem. Eng.*, 3, 240 (1958).
2. Bernard, R. A., and R. H. Wilhelm, *Chem. Eng. Progr.*, 46, 233 (1950).
3. Cairns, E. J., Dissertation, Univ. Calif., Berkeley (1959).
4. ———, and J. M. Prausnitz, *Ind. Eng. Chem.*, 51, 1441 (1959).
5. ———, *A.I.Ch.E. Journal*, 6, 3, 400 (1960).
6. Danckwerts, P. V., *Appl. Sci. Res.*, 3, 279 (1952).
7. Dryden, H. L., *Ind. Eng. Chem.*, 31, 416 (1939).
8. Gilliland, E. R., and E. A. Mason, *ibid.*, 41, 1191 (1949).
9. ———, *ibid.*, 44, 218 (1952).
10. Hanratty, T. J., George Latinen, and R. H. Wilhelm, *A.I.Ch.E. Journal*, 2, 372 (1956).
11. ———, *ibid.*, 2, 42 (1956).
12. Hinze, J. O., "Turbulence," Chap. 5, McGraw-Hill, New York (1959).
13. Kalinske, A. A., and C. L. Pien, *Ind. Eng. Chem.*, 36, 220 (1944).
14. Klinkenberg, A. R., *et al.*, *ibid.*, 45, 1202 (1953).

14a. Lemlich, Robert, and Isidoro Coldas, Jr., *A.I.Ch.E. Journal*, 4, 376 (1958).

15. Leva, Max, *et al.*, *Ind. Eng. Chem.*, 41, 1206 (1949).
16. Morse, R. D., *ibid.*, 1117 (1949).
17. Prausnitz, J. M., and R. H. Wilhelm, *ibid.*, 49, 978 (1957).
18. Taylor, G. I., *Proc. London Math. Soc.*, 20, 196 (1921).
19. ———, *Proc., Roy. Soc. (London)*, 151A, 421 (1935).
20. Towle, W. L., and T. K. Sherwood, *Ind. Eng. Chem.*, 31, 457 (1939).
21. Wilde, Douglass J., M.S. thesis, Univ. Wash., Seattle (1956).

Manuscript received March 19, 1959; revision received October 30, 1959; paper accepted November 2, 1959.